Multifunctional epoxy/carbon fiber laminates for thermal energy storage and release

Giulia Fredi*, Andrea Dorigato, Luca Fambri and Alessandro Pegoretti*

University of Trento, Department of Industrial Engineering and INSTM Research Unit
via Sommarive 9 - 38123 Trento, Italy

*Corresponding authors: **giulia.fredi@unitn.it; alessandro.pegoretti@unitn.it**

Abstract

This work is focused on the preparation and characterization of novel multifunctional structural composites with thermal energy storage (TES) capability. Structural laminates were obtained by combining an epoxy resin, a paraffinic phase change material (PCM) stabilized with carbon nanotubes (CNTs), and reinforcing carbon fibers. The stabilized paraffin kept its ability to melt and crystallize in the laminates, and the melting enthalpy of the composites was proportional to the paraffin weight fraction with a maximum value of 47.4 J/cm^3. This thermal response was preserved even after fifty consecutive heating-cooling cycles. Moreover, the thermal conductivity of the laminates through thickness direction resulted to increase proportionally to the content of CNT-stabilized PCM. The capability of the developed TES laminates to contribute to the thermal energy management was also proven by monitoring their cooling rates through thermal imaging. The flexural modulus was only slightly affected by the presence of the PCM, while a decrease of flexural strength, strain at break and interlaminar shear strength was detected. Optical microscopy highlighted that this could be attributed to the preferential location of the PCM in the interlaminar region. The obtained results demonstrated the feasibility of the concept of multifunctional structural TES composites.

Keywords: multifunctional composites; thermal properties; polymer-matrix composites (PMCs); carbon nanotubes; carbon fibers.

1. Introduction

Thermal energy storage (TES) can be defined as the temporary storage of excess heat and waste energy for a later use. This is advantageous as it allows leveling the difference between heat supply and request. Materials involved in TES technologies can be classified in sensible heat, latent heat and thermochemical heat TES systems [1].Among the latent heat systems , solid-liquid organic phase change materials (PCMs) can store a large amount of heat per unit mass thanks to their high specific phase change enthalpy, and thus they can efficiently accumulate and release latent heat for TES applications. Moreover, they can operate in a precise temperature range with small volume variation [2, 3]. The most common PCMs are paraffin waxes, poly(ethylene glycol)s and fatty acids [4]. Despite their advantages, they are all characterized by a relatively low thermal conductivity and leakage problems when they are in the molten state [5]. The leakage can be limited in two main ways, i.e. through micro/nano-encapsulation of the PCMs in organic or inorganic shells [6], and through the confinement in a polymer network or in a porous or layered structure [7, 8]. This second method is called “shape-stabilization”, and if it is achieved with a thermally conductive material, such as a carbon-based nanofiller, it also may help to overcome the problem of the low thermal conductivity of organic PCMs, thus improving the overall thermal exchange [3, 9, 10]. PCMs find application in many different fields, such as the building industry [9, 11, 12], hot or cold water storage [13, 14], and solar thermal energy collection [14, 15]. They can also be used to produce smart thermo-regulating garments [16-18] or employed in the cooling of electronic devices [19]. However, in most of the mentioned applications, TES systems represent a supplementary component to be added to the main structure, but, in applications where weight and volume savings are critical design parameters, it would be beneficial to embed energy storage/management functionalities directly into structural materials. In this context, polymer-matrix composites have the potentialities to be designed as

multifunctional materials with both structural and non-structural functions [20-23]. Lightweight polymer composites combining high mechanical properties and TES capability could find applications in different areas, such as the automotive industry, where the diffusion of lightweight structures could complicate the thermal management of the environment in the cockpit, or the portable electronics field, where the reduction of volumes and masses also limits the space available for the cooling system. Although there are many examples in the literature of composites constituted by a PCM and a shape-stabilizing agent (carbon-based, organic, ceramic or metallic), up to now little has been done to produce and characterize polymer-matrix structural composites with TES capacity. Wirtz et al. [24] developed a multifunctional sandwich composite based on a graphitic core impregnated with paraffin embedded in two carbon fiber/epoxy composite skins. In this material, thought to ease the cooling of electronic devices, the graphitic core effectively stabilizes the paraffin and increases the thermal conductivity of the sandwich core, while the carbon/epoxy skins improve the overall mechanical performance. More recently, Yoo et al. [25, 26] added TES function to glass-fiber reinforced laminates by including a microencapsulated PCM in the epoxy matrix, and investigated their thermal and mechanical properties. The phase change transitions of the microcapsules preserved after their incorporation in the laminate, while the tensile and flexural stiffness and strength of the laminates decreased upon PCM addition. In the flexural tests, delamination and matrix cracking increased with an increase of microcapsules, and the authors underlined the importance of improving the adhesion between epoxy and microcapsules. Even though the work of Yoo et al. highlights the potentialities of multifunctional laminates containing PCMs, the use of glass fibers, which have a density higher than other fibers like carbon or polyethylene, do not allow the maximization of the matrix weight fraction and thus the PCM content in the laminate, and do not contribute significantly to the thermal conductivity of the composite.

The aim of this work was the production and the characterization of novel epoxy/carbon structural laminates having the capability to store and release thermal energy in a certain temperature range and in a cyclic-reversible durable manner. This has been achieved by combining an epoxy resin with continuous carbon fibers and a paraffin wax shape-stabilized with carbon nanotubes (CNTs). As mentioned before, these systems differentiate from other similar systems for the use of carbon fibers, which have a low density and allow the maximization of the weight fraction of the matrix, the true multifunctional component. Moreover, the use of a shape-stabilized PCM (instead of a microencapsulated one) to add TES properties to a traditional composite laminate has not been addressed before, to the best of the authors' knowledge. The epoxy/wax/CNT blends have been developed and presented in a previous paper of our group, focused on the shape-stabilizing properties of CNTs for paraffin and on the effect of the paraffin and CNT amount on the mechanical, thermal and electrical properties of the epoxy resin [27]. In the present work, these epoxy/wax/CNT blends were used to prepare laminates with a balanced plain-weave carbon fiber fabric, and the thermal and mechanical properties of these laminates were extensively investigated.

2. Materials and methods

2.1 Materials

RT44HC® paraffin wax (melting temperature = 44 °C, density = 0.8 g/cm^3) was supplied by Rubitherm Technologies GmbH (Germany). Multi-walled CNTs NC7000® (average diameter 9.5 nm, average length 1.5 µm, BET surface area 250-300 m^2/g) were purchased from Nanocyl SA (Belgium). The epoxy base Elan-tech® EC 157 (density = 1.15 g/cm^3, viscosity at 25 °C = 550 mPa·s) and the hardener Elan-tech® W 342 (density = 0.95 g/cm^3, viscosity at 25 °C = 50 mPa·s) were kindly provided by Elantas Europe s.r.l. (Italy). Balanced plain weave carbon fabric Angeloni GG200P (mass per unit area = 192 g/m^2) made of intermediate modulus carbon fibers

(3000 fibers per tow, linear density = 200 tex) was purchased from G. Angeloni s.r.l. (Italy). A plain fabric was preferred over other types of weaves (e.g. twill or satin), because it has the highest number of interlaces between warp and weft, which helps in maintaining the geometry of the fabric and minimizes any undesired fiber waviness during the fabrication process [28]. All the materials were used as received.

2.2 Sample preparation

The shape stabilized PCM was prepared as described in a previous work of our group [27]. Briefly, CNTs were added to the molten paraffin wax at 70 °C and mechanically stirred at 500 rpm for 30 minutes. The CNT:paraffin weight ratio was 1:9, since this is the minimum amount of CNTs at which no leakage of paraffin was detected above its melting temperature. The mixture was then cooled down to room temperature and grinded in a cryogenic blade miller Ika Laborteknik M20. Figure 1(a-b) shows an optical microscope image of the paraffin-CNTs powder (obtained with a Wild Heerbrugg optical microscope equipped with an Allied Pike F032 camera) and the particle size distribution obtained through a dimensional analysis with ImageJ® software.

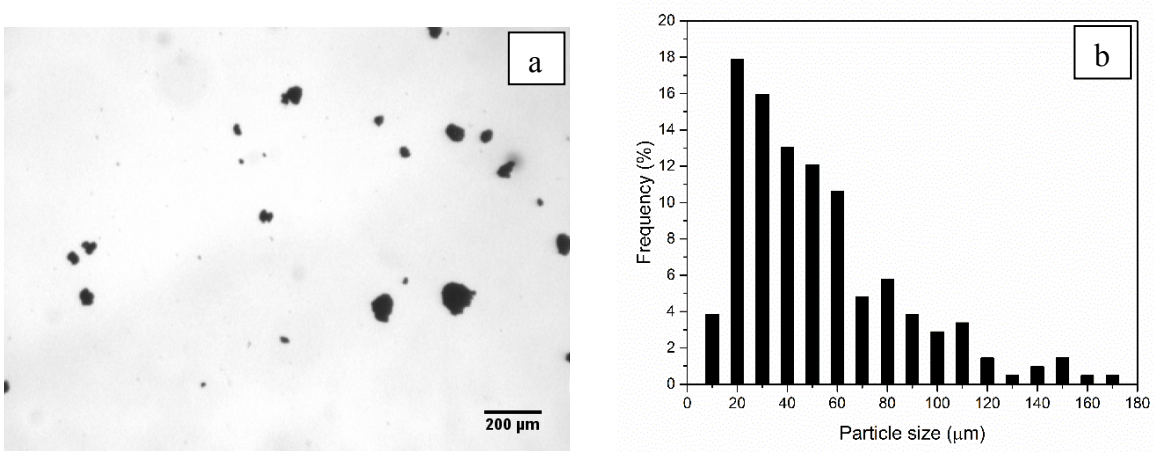

Figure 1. (a) Optical microscope image and (b) particle size distribution of paraffin-10wt% CNTs powder obtained through cryogenic blade milling.

The particles had an average size of 53 ± 30 µm, and were denoted as ParCNT. The epoxy base and the hardener were mixed at room temperature at a weight ratio of 100:30, as suggested by the producer, and magnetically stirred at 500 rpm for 5 minutes. The ParCNT powder was then added at different weight concentrations (i.e. 20%, 30% or 40%), and the resulting mixture was vigorously stirred to obtain a homogeneous dispersion of the powder in the resin. Laminates were produced via wet lay-up method and the relative amounts of components were chosen to obtain a nominal fiber weight fraction of 50%. Five plies were stacked together, and the resulting laminates had an in-plane area of 120 x 120 mm^2. The laminates were vacuum-bagged, left to cure at room temperature for 24 hours and post cured at 100 °C for 10 hours in a hot-plate press under a pressure of 0.8 MPa. A carbon fiber/epoxy laminate without paraffin and CNTs was prepared following the same procedure. Table 1 displays the list of prepared laminates, with the nominal weight fractions of constituents. The composites were denoted as EP-ParCNTx-CF, where x represents the weight percentage of paraffin-CNTs powder with respect to the total mass of the matrix. As mentioned before, x assumes the values of 20%, 30% and 40%.

Table 1. List of prepared laminates with the nominal weight fractions of the constituents.

Sample	Carbon fibers (wt%)	Epoxy (wt%)	Paraffin (wt%)	CNTs (wt%)
EP-CF	50	50	0	0
EP-ParCNT20-CF	50	40	9	1
EP-ParCNT30-CF	50	35	13.5	1.5
EP-ParCNT40-CF	50	30	18	2

2.3 Experimental techniques

2.3.1 Density of the laminates and fraction of constituents

To measure the mass fraction of the constituents, each laminate was weighted and the mass of the fibers, which is known from the area of the composite and the mass per unit area of the fabric, was subtracted from the total weight. The obtained fiber-to-matrix mass ratio was then compared to that obtained through thermogravimetric analysis (see Par. 2.3.3). The experimental density of the carbon fiber fabric, the matrices (with a various amount of paraffin-CNTs) and the laminates was measured with the technique of the Archimedes balance in ethanol [29], through a Gibertini E42 analytical balance. Thus, a theoretical and an experimental density could be obtained, and the volume fractions of fibers, matrix and voids were subsequently calculated.

2.3.2 Microstructural analysis

Optical microscope micrographs were acquired on polished samples at different magnifications, with an upright incident-light optical microscope Zeiss Axiophot, equipped with Epiplan Neofluar objectives. Scanning Electron microscopy (SEM) micrographs of the cryofractured surfaces of all the laminates were acquired through a Jeol IT300 scanning electron microscope, after Pt-Pd sputtering.

2.3.3 Thermal analysis

Thermogravimetric analysis (TGA) was performed with a Mettler TG50 instrument. Samples of approximately 25 mg were tested at a heating rate of 10 °C/min up to 700 °C, under a nitrogen flow of 150 ml/min. With this test, the degradation temperatures of the different components were investigated, and experimental weight fractions of paraffin and epoxy resin in the laminates were determined. The temperatures associated to a mass loss of 3% ($T_{3\%}$) was also computed.

Differential scanning calorimetry (DSC) tests were performed with a Mettler DSC30 machine in a temperature interval between 0 °C and 150 °C, at a heating/cooling rate of 10 °C/min, under

a nitrogen flow of 100 ml/min. All the specimens, with a mass of approximately 20 mg each, underwent a first heating scan, a cooling scan and a second heating scan. Through these tests, it was possible to measure the melting and crystallization temperatures (T_m, T_c) and the phase change enthalpy values ($\Delta H_m, \Delta H_c$) of the paraffin wax, and the glass transition temperature (T_g) of the epoxy resin. As reported in our previous paper [27], relative melting and crystallization enthalpy values ($\Delta H_m^{rel}, \Delta H_c^{rel}$) were determined for the laminates normalizing ΔH_m and ΔH_c to the weight fraction of paraffin, as reported in Equations 1 and 2:

$$\Delta H_m^{rel} = \frac{\Delta H_m / w_p}{\Delta H_m^{neat}} \quad (1)$$

$$\Delta H_c^{rel} = \frac{\Delta H_c / w_p}{\Delta H_c^{neat}} \quad (2)$$

where w_p is the weight fraction of paraffin and ΔH_m^{neat} and ΔH_c^{neat} are the specific melting and crystallization enthalpies of neat paraffin, respectively. The retention of the thermal energy storage/release capability was assessed through cyclic DSC test. The tests were performed between 10 °C and 70 °C at 10 °C/min, under a nitrogen flow of 100 ml/min. The same DSC tests were performed also on the ParCNT powder, to verify that the thermal properties of the PCM were not impaired by the cryomilling process.

Thermal conductivity and diffusivity values were obtained through laser flash analysis (LFA) using a Netzsch LFA 447 device. Square specimens with an edge length of 12.7 mm were cut from the laminates. Measurements were performed by exposing one side of the sample to an energy pulse from a light source, and measuring the temperature history on the other side. At least two specimens were tested for each composition. Each specimen was tested at four temperatures (25, 35, 45 and 55 °C), and 3 pulses were performed for each temperature. Data were analyzed using the software Proteus. Thermal diffusivity (α) was calculated using the Cowan method with pulse correction. For the determination of the heat capacity (c_P), the

reference material Pyrex 7740, prepared according to ASTM-E 1461, was measured and compared with the samples. The thermal conductivity (λ) was calculated as reported in Equation 3:

$$\lambda = \alpha \rho c_p \qquad (3)$$

where ρ is the sample density, measured as described in paragraph 2.3.1. All the values of thermal conductivity were calculated using the sample density calculated at room temperature; this is acceptable, since the investigated temperature range is small, and the molten material is confined and is a small weight fraction of the whole specimen.

Finally, a simple test was performed to check the overall thermal performance of the laminates. Rectangular specimens with a surface area of 70 x 100 mm^2 were cut from the laminates with a diamond wheel. Each specimen was heated in an oven at 60°C for 30 minutes, then taken out and left cooling down to room temperature under laboratory conditions. During the cooling phase, the surface temperature was recorded with an infrared thermal imaging camera (FLIR E60).

Dynamic mechanical thermal analysis (DMTA) was performed with a TA Q800DMA instrument in single cantilever bending mode. The specimens had nominal dimensions of 35x5x1.3 mm^3 and the distance between the grips was fixed at 17.5 mm. Storage modulus, loss modulus and tanδ were measured in the range 0-180 °C at 3 °C/min, with a strain of 0.05% applied at a frequency of 1 Hz.

2.3.4 Mechanical testing

Three-point flexural tests were performed according to ASTM D790-03 standard, with an Instron 5969 universal testing machine, equipped with a 50 kN load cell. The nominal dimensions of the tested specimens were 120x10x1.3 mm^3. A diamond wheel was used to cut the specimens out of

the prepared laminates. The span length was fixed at 85 mm and the crosshead speed was adjusted for each specimen in order to have a strain rate on the outer side of the specimens of 0.01 mm/mm. At least five specimens were tested for each sample. The tangent modulus of elasticity (E), the flexural strength (σ_{fM}) and the flexural strain at break (ε_b) were determined for each specimen with Equations 4, 5 and 6, as:

$$E = L^3 m / 4bd^3 \quad (4)$$

$$\sigma_{fM} = \frac{3PL}{2bd^2}\left[1 + 6\left(\frac{D}{L}\right)^2 - 4\left(\frac{D}{L}\right)\left(\frac{d}{L}\right)\right] \quad (5)$$

$$\varepsilon_b = 6Dd/L^2 \quad (6)$$

where L is the support span, m is the slope of the tangent to the initial portion of the load-deflection curve, b and d are the specimen width and thickness, P is the maximum load and D is the deflection at the break point. For the evaluation of the flexural strength in specimens tested at high span-to-thickness ratios, the standard suggests the formula in Equation 5, to consider the not negligible forces developed at the supports. It should be noted that the flexural strength in Equation 5 is based on the classical beam theory, which assumes a linear stress distribution through the specimen thickness, which is not fully correct for laminates. Thus, the resulting flexural strength is an apparent flexural strength, which is still useful for comparison purposes, to evaluate the maximum load that the laminate can bear, at a given thickness and span [30].

Short-beam shear (SBS) tests were performed to evaluate the interlaminar shear strength of the prepared laminates [31], following the ASTM D 2344 standard, with an Instron 5969 universal testing machine equipped with a 50 kN load cell. The nominal dimensions of the tested specimens were 15x5x2 mm^3. A diamond wheel was used to cut the specimens out of the prepared laminates. The span length was fixed at 8 mm and the crosshead speed was 1 mm/min. The short-beam interlaminar shear strength, F^{sbs}, was calculated as $F^{sbs} =$

$(0.75\,P_m\,)/(bh)$, where P_m is the maximum load and b and h are the specimen width and thickness, respectively. At least five specimens were tested for each sample. Also this equation is derived from the classical beam theory, which assumes that the shear stress is parabolically distributed in the cross-section of the specimen, but, as thoroughly studied in the literature, the shear behavior of composite laminates deviates markedly from linearity and the maximum shear stress is significantly lower than that predicted by this theory [31]. Although the real shear strength is expected to be lower than that calculated as mentioned above, the apparent value can be considered suitable for this work, as it is used only for comparison [31].

3. Results and discussion

3.1 Density of the laminates and fraction of constituents

Table 2 reports the experimental weight fraction of fibers, the experimental density of the laminates and the calculated volume fraction of the constituents. The thickness of the laminates is also reported.

Table 2. Fiber content (wt and vol %), experimental density, porosity and thickness of the laminates.

Sample	Fibers (wt%)	Fibers (vol%)	Density (g/cm^3)*	Pores (vol%)	Thickness (mm)
EP-CF	50.7 ± 0.7	40.4 ± 0.7	1.384 ± 0.004	5.1 ± 0.2	1.46 ± 0.03
EP-ParCNT20-CF	49.2 ± 0.6	37.0 ± 1.2	1.323 ± 0.011	5.7 ± 0.8	1.67 ± 0.05
EP-ParCNT30-CF	48.9 ± 0.3	35.4 ± 1.8	1.295 ± 0.021	5.5 ± 1.5	1.65 ± 0.07
EP-ParCNT40-CF	52.2 ± 0.4	37.8 ± 0.9	1.303 ± 0.012	5.8 ± 0.9	1.57 ± 0.03

* temperature = 22.1 °C; density of Et-OH 96 vol% = 0.7995 g/cm^3 [29].

The experimental fiber weight fraction is approximately 50% for all the laminates, i.e. close to the nominal fraction. Because of the different viscosities and densities of the prepared matrices, during the production of the laminates it is difficult to obtain exactly the same fiber volume fraction in all the samples. Also, small variations in the fiber volume fraction are common and usually accepted for laminates produced with matrices with different composition and viscosity [28]. As shown in Table 2, the fiber volume fractions are similar, which allows a proper comparison between the mechanical properties of the different laminates. Moreover, the volume fraction of pores of the prepared composites is approximately 5 %, and this void concentration could be considered high for the production of structural components [32]. Nevertheless, it is the same for laminates with different compositions, and a comparison of the mechanical properties of the laminates is therefore possible The obtained fiber volume fraction is rather low with respect to traditional structural composites [33], but it is compatible with the hand lay-up process, compared with previous studies [34-37]. Moreover, for the production of the multifunctional composites object of this work, a low fiber volume and weight fraction leads to a high matrix fraction, which enhances the thermal energy storage properties of the laminates.

3.2 Microstructural analysis

The optical microscope images of the prepared laminates are shown in Figure 2(a-f). It can be clearly seen that the paraffin-CNTs particles tend to aggregate, probably because of the compaction pressure and temperature applied during the curing and the post-curing steps. The PCM phase is mainly distributed in the interlaminar zones between two subsequent fiber layers, while the portion of matrix infiltrating the tows and wetting each single fiber is almost exclusively composed by epoxy resin. This is mainly due to the size of PCM particles (about 50 μm at the beginning of the production process). Thus, the interlaminar zone is enriched in PCM,

which is present in a weight fraction superior to the nominal one in these regions. This is even more clearly visible in Figure 2(e-f), taken at higher magnifications. Additionally, since the paraffin-CNTs domains are solid in the first part of the curing process at room temperature, they tend to deform the tows. To have a more detailed analysis of the microstructural behavior of the prepared laminates, the SEM micrographs at different magnifications of the cryofractured surface of the EP-CF (Figure 3(a-b)) and EP-ParCNT40-CF (Figure 3(c-d)) samples are reported. These SEM micrographs confirm that there are no evident traces of paraffin-CNTs particles between the fibers, as suggested by the fact that there are no noticeable microstructural differences between Figure 3b and Figure 3d. The differences are instead clearly visible between the interlaminar zones of the two laminates; in Figure 3c the interlaminar zone (indicated by some red arrows) is rich in ParCNT, which is not present in the EP-CF sample (Figure 3a).

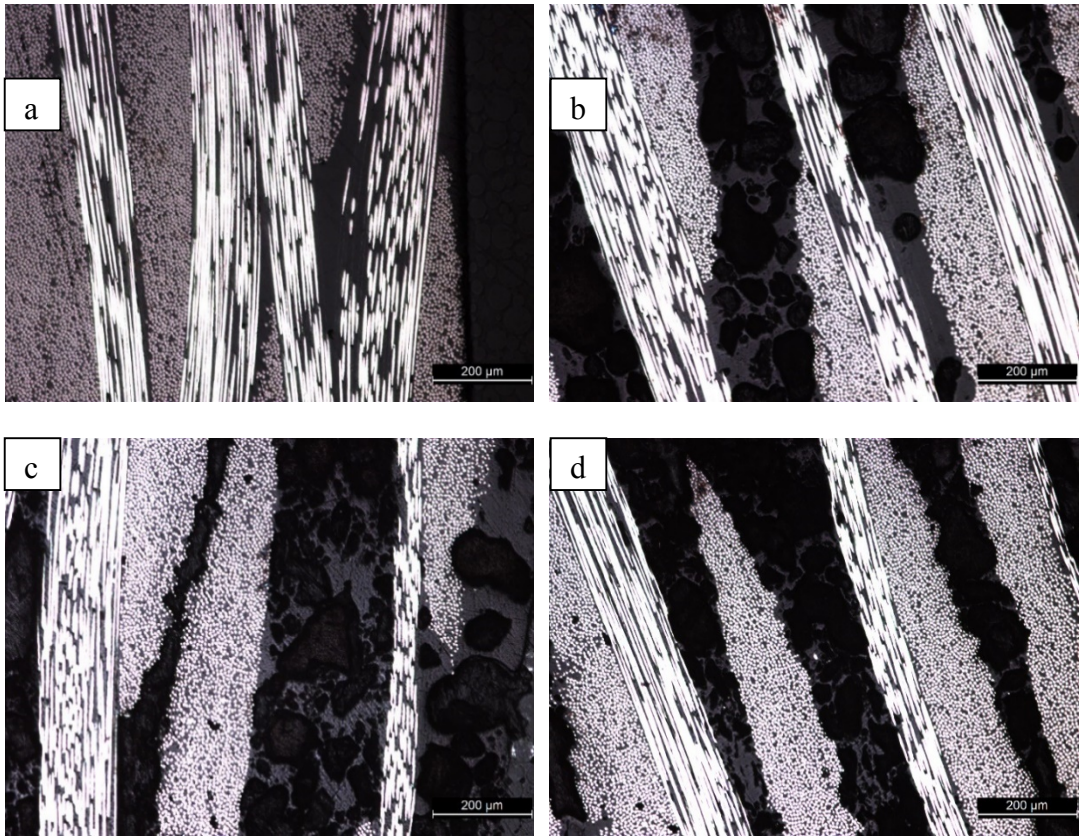

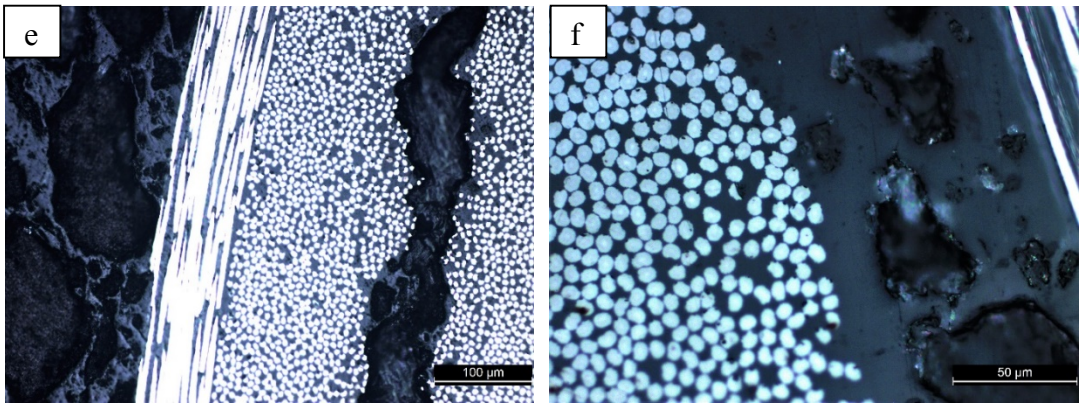

Figure 2. optical microscope images of the prepared laminates. (a) EP-CF; (b) EP-ParCNT20-CF; (c) EP-ParCNT30-CF; (d) EP-ParCNT40-CF; (e) and (f) EP-ParCNT30-CF at higher magnification.

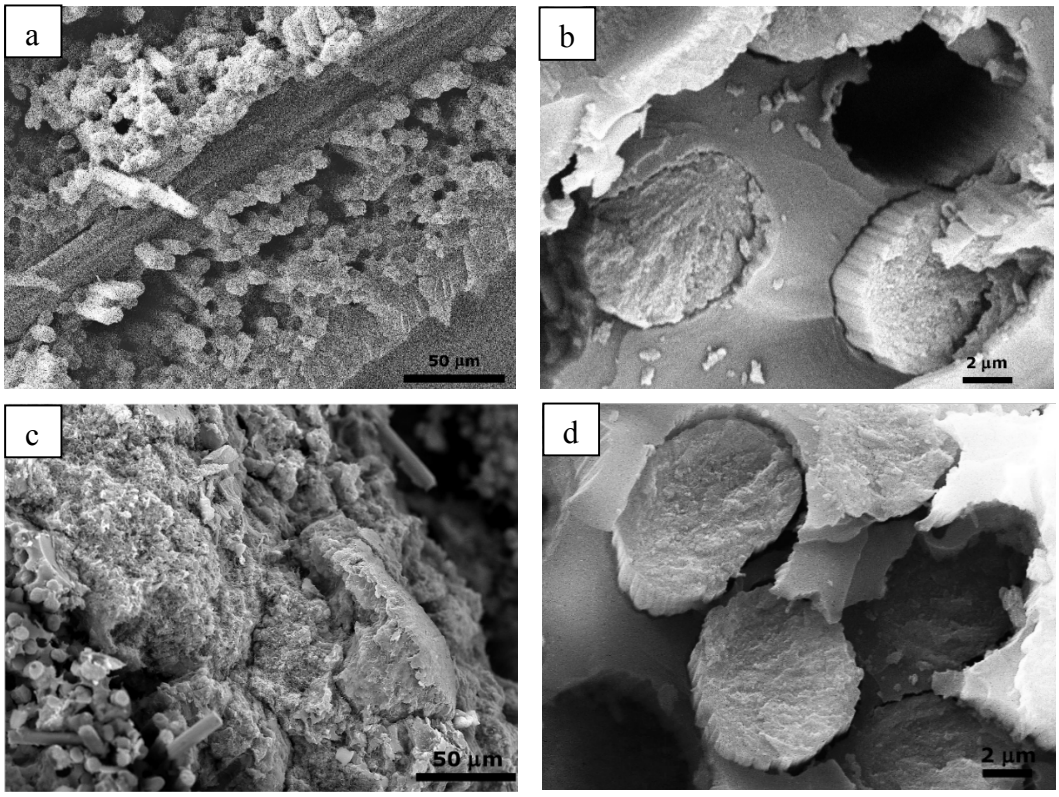

Figure 3. SEM micrographs of the cryofractured surface of the laminates. (a, b) EP-CF and (c, d) EP-ParCNT40-CF samples. The red arrows in Figure 3c indicate the ParCNT-rich zone.

3.3 Thermal analysis

Figure 4 reports the TGA thermograms of the laminates, compared with that of the neat epoxy resin, the carbon fibers and the ParCNT particles. As observed in our previous work [27], the

degradation of the polymeric fraction of the samples happens in two distinct steps, which can be associated to the degradation of paraffin and the epoxy resin, at approximately 230 °C and 380 °C, respectively. The mass residue after the test is mainly represented by carbon fibers and CNTs, but it also partly consists of epoxy resin, as the thermogram of the neat epoxy demonstrates. From the degradation profile of the neat paraffin it is possible to determine an experimental mass fraction of paraffin in the samples, also considering the mass loss from the epoxy. From the residues, matrix and fiber weight fractions could be determined for all the samples. These values, reported in Table 3, are close to the nominal ones reported in Table 1. After the determination of the weight fractions of paraffin and epoxy in the laminates, the paraffin-to-epoxy ratio was calculated.

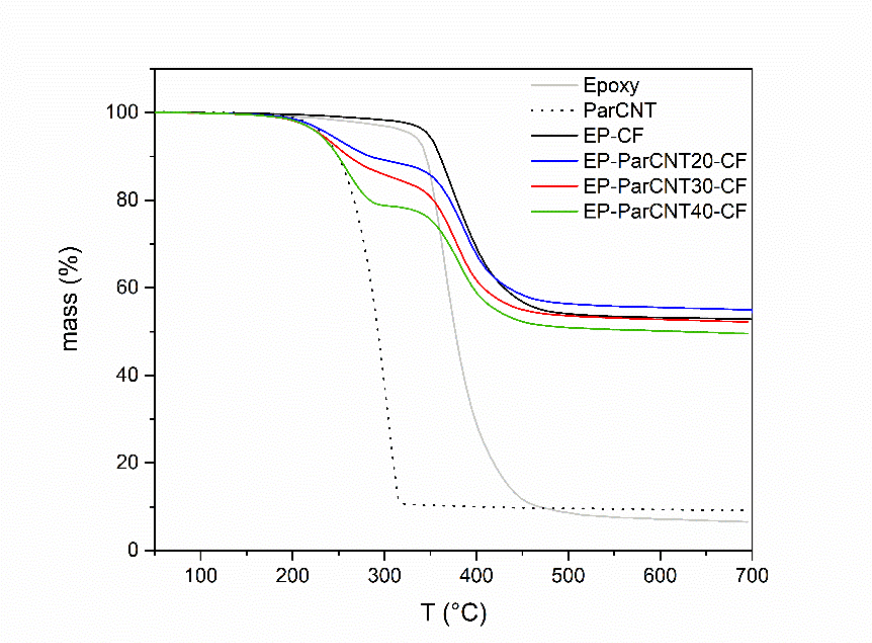

Figure 4. TGA thermograms of the laminates, of neat epoxy and of ParCNT particles.

Table 3. Results of TGA tests on the laminates.

Sample	$T_{3\%}$ (°C)	Paraffin (wt%)	Paraffin-to-Epoxy ratio	Paraffin-to-Epoxy nominal ratio	Fibers (wt%)
EP-CF	333.4	0	0	0	50.0
EP-ParCNT20-CF	222.8	9.02	0.237	0.225	51.6
EP-ParCNT30-CF	215.0	12.78	0.345	0.386	48.2
EP-ParCNT40-CF	208.3	19.52	0.598	0.600	49.2

From Table 3 it can be seen that also this value is close to the nominal one, which suggests that not only is the total paraffin content preserved, but also the relative amount of the components in the matrix. The weight fraction of fibers is comparable to that found with the method described in paragraph 2.3.1 and reported in Table 2. As expected, paraffin addition leads to a lowering of the thermal degradation resistance of the laminates, with a decrease of the $T_{3\%}$ values.

The DSC thermograms on the laminates during the first heating scan and the cooling scan are reported in Figure 5(a-b). The most important parameters obtained from these tests are summarized in Table 4.

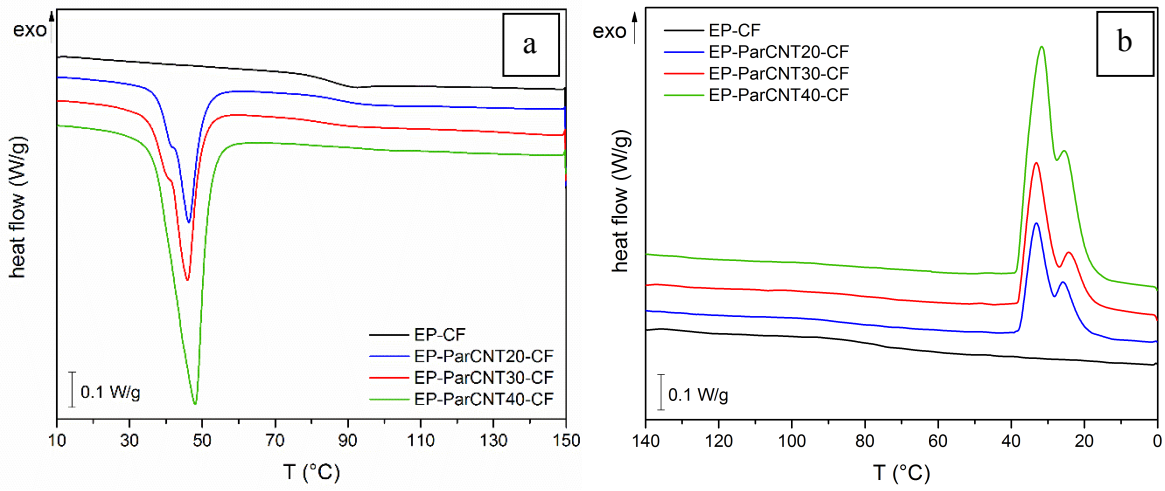

Figure 5. DSC thermograms of the laminates. (a) first heating scan; (b) cooling scan.

The values of melting and crystallization enthalpies of the ParCNT powder are proportional to the nominal weight fraction of paraffin (the values of ΔH_m^{rel} and ΔH_c^{rel} are nearly 100%), which suggests that the presence of CNTs and the cryomilling process do not impair the thermal properties of the PCM. From the tests on the laminates, it emerges that the glass transition temperature of the epoxy is practically not affected by the presence of the PCM, and the T_m of the paraffin is not influenced by the presence of the epoxy. The effect of the production process of the laminates on the phase change enthalpies of the PCM can be evaluated considering the values of relative enthalpies ($\Delta H_m^{rel}, \Delta H_c^{rel}$), which are in the range of 80-90%. Values in this range were found also during the characterization of the neat matrices reported in our previous work [27] and in different literature works where a paraffinic PCMs was confined in a polymer matrix [38, 39]. This can be due to a non-homogeneous distribution of the paraffin, to the confinement of the PCM molecules by the presence of the surrounding matrix, or to a partial dissolution of the paraffin in the polymer matrix [38, 39], but further tests will be needed to fully understand this aspect. Also, this can be because part of the paraffin degrades or exudates out of the sample during the fabrication, but this is probably not the case of this work, or at least not the main cause, since the weight fractions of paraffin calculated from the TGA analysis are close to the nominal ones (see Table 1 and Table 3).

Table 4. Results of DSC tests on neat paraffin, on ParCNT powder and on the laminates.

Sample	T_g (°C)	T_m (°C)	ΔH_m (J/g)	ΔH_m^{rel} (%)	ΔH_m (J/cm^3)	T_c (°C)	ΔH_c (J/g)	ΔH_c^{rel} (%)
Neat paraffin	-	44.5	242.1	100	193.7	35.0	241.2	100
ParCNT	-	43.8	216.8	99.5	194.0	34.2	215.5	99.4
EP-CF	84.0	-	-	-	-	-	-	-

EP-ParCNT20-CF	85.7	45.0	20.3	91.5	26.9	34.3	19.5	88.6
EP-ParCNT30-CF	82.1	43.8	27.3	81.8	35.4	35.0	26.3	79.1
EP-ParCNT40-CF	82.0	45.1	36.4	87.4	47.4	33.9	36.2	87.3

$\boldsymbol{T_g}$ = glass transition temperature of the epoxy resin; $\boldsymbol{T_m}$, $\boldsymbol{T_c}$= melting and crystallization temperatures of ParCNT; $\Delta\boldsymbol{H_m}$, $\Delta\boldsymbol{H_c}$= melting and crystallization enthalpies of ParCNT; $\Delta\boldsymbol{H_m^{rel}}$, $\Delta\boldsymbol{H_c^{rel}}$= relative melting and crystallization enthalpies of ParCNT;

Cyclic DSC tests were performed on all samples with the PCM to evaluate the retention of the thermal energy storage/release effect over cyclic conditions. Only the results obtained on the EP-ParCNT40-CF sample are reported for the sake of brevity. Figure 6 shows representative DSC thermograms of the 1st, 30th and 50th thermal cycles.

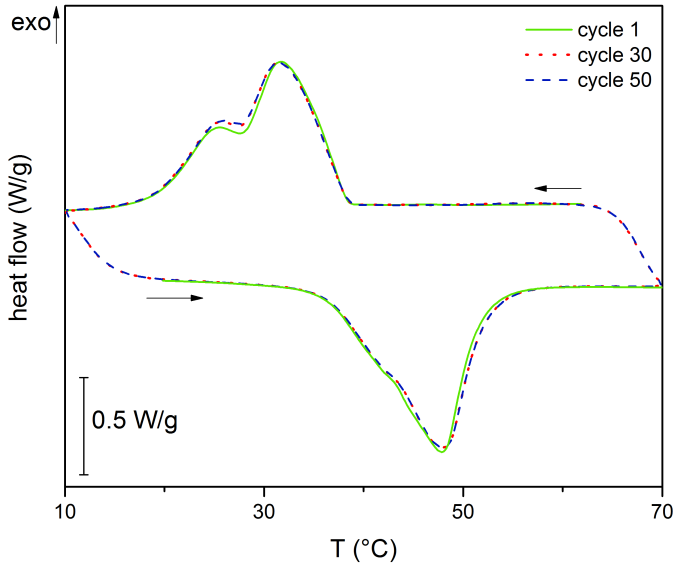

Figure 6. DSC thermograms of the 1st, 30th and 50th cycles on EP-ParCNT40-CF.

The thermograms at different cycles are overlapped, and there are no appreciable differences in the phase change temperatures and enthalpies measured at different cycles. This suggests that the thermal properties of the laminates are stable up to fifty cycles in the analyzed temperature

range, which is an indication of the thermal reliability of the prepared composites. To fully study this aspect, cyclic tests of heating and cooling of a laminate in environmental conditions are needed.

The values of thermal diffusivity, specific heat and thermal conductivity of the investigated laminates are reported in Figure 7(a-c). Each column represents the mean value and the standard deviation of all the measurements performed on each composition (at least two specimens, three pulses each). The values observed for the sample without paraffin (EP-CF) are compatible with similar measurements found in literature for polymer-matrix composites analyzed in the thickness direction [40, 41]. For the laminate without paraffin (EP-CF), the diffusivity does not change significantly with temperature, while the specific heat and the thermal conductivity slightly increase. For the laminates containing paraffin, the trends of specific heat and thermal conductivity show a maximum at 35°C, as the PCM is approaching the solid-liquid phase change, as already observed in the literature [42]. For these laminates, at a given temperature the values of thermal conductivity and diffusivity increase with the content of ParCNT, probably due to the presence of the CNTs used as stabilizing fillers. The results of this test are important as they show that the addition of a CNT-stabilized PCM positively increase the thermal conductivity through the thickness of a carbon/epoxy laminate, both in the solid and in the liquid state.

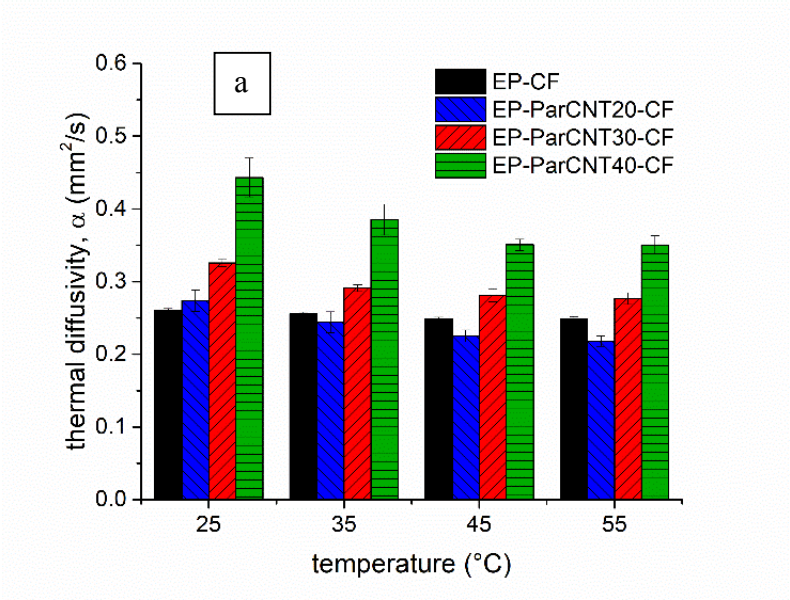
a
EP-CF
EP-ParCNT20-CF
EP-ParCNT30-CF
EP-ParCNT40-CF
thermal diffusivity, α (mm²/s)
0.0
0.1
0.2
0.3
0.4
0.5
0.6
25
35
45
55
temperature (°C)

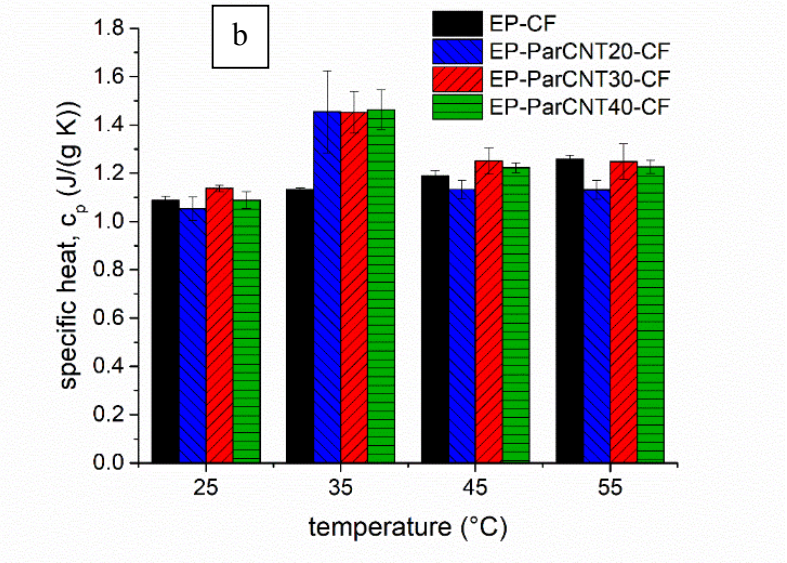
b
EP-CF
EP-ParCNT20-CF
EP-ParCNT30-CF
EP-ParCNT40-CF
specific heat, cp (J/(g K))
0.0
0.2
0.4
0.6
0.8
1.0
1.2
1.4
1.6
1.8
25
35
45
55
temperature (°C)

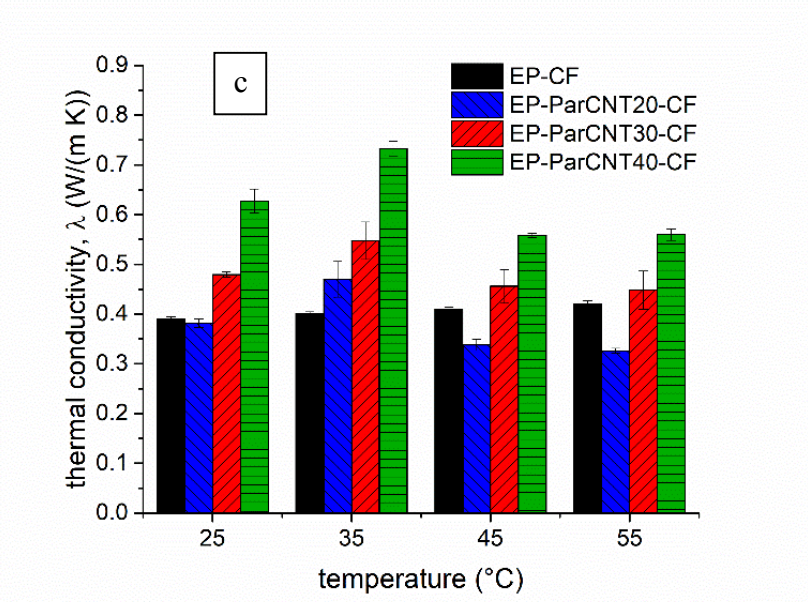

Figure 7. Results of the laser flash analysis measurements: (a) thermal diffusivity; (b) specific heat; (c) thermal conductivity.

Figure 8 reports the results of the thermal imaging test. The starting temperature is lower than 60°C because the laminates slightly cooled down during the time required to take them out of the oven to begin the measurement, but it is still above the onset crystallization temperature of the PCM.

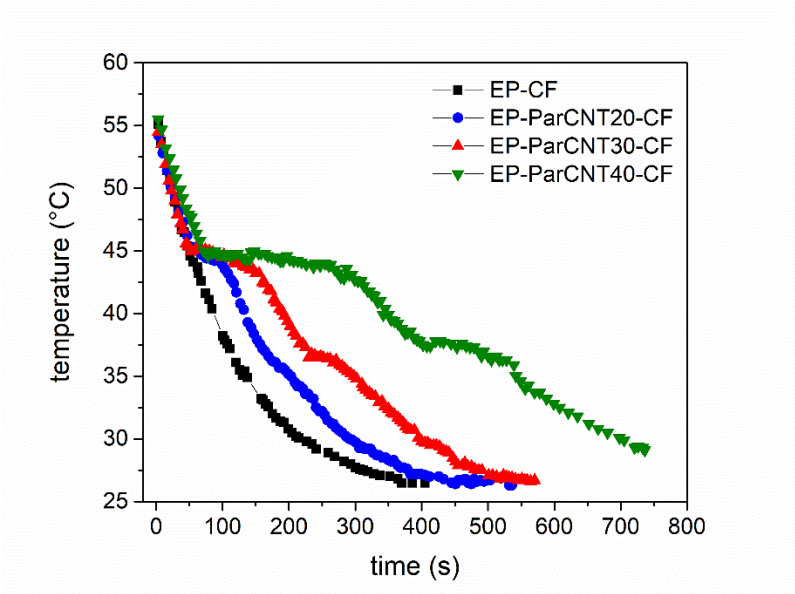

Figure 8. Surface temperature of the laminates as a function of time during cooling at room temperature.

In the laminates containing the PCM the temperature decreases with a plateau-like trend induced by the heat released during the crystallization of PCM, which is not the case for neat EP-CF laminate. As a consequence, the cooling time increases considerably. For example, the time required to reach 30°C is of about 200 s for the EP-CF laminate and increases up to about 700 s for the EP-ParCNT40-CF laminate. Although this is a simple test and it investigates only the cooling phase, it clearly highlights the remarkable differences in the thermal behavior of the laminates as a function of the PCM content.

The results of the DMTA tests are presented in Figure 9(a-b), with the trends of the storage modulus and the loss modulus as a function of temperature and the values of the storage modulus at 30 °C and 70 °C as a function of the specific volumetric enthalpy of the laminates.

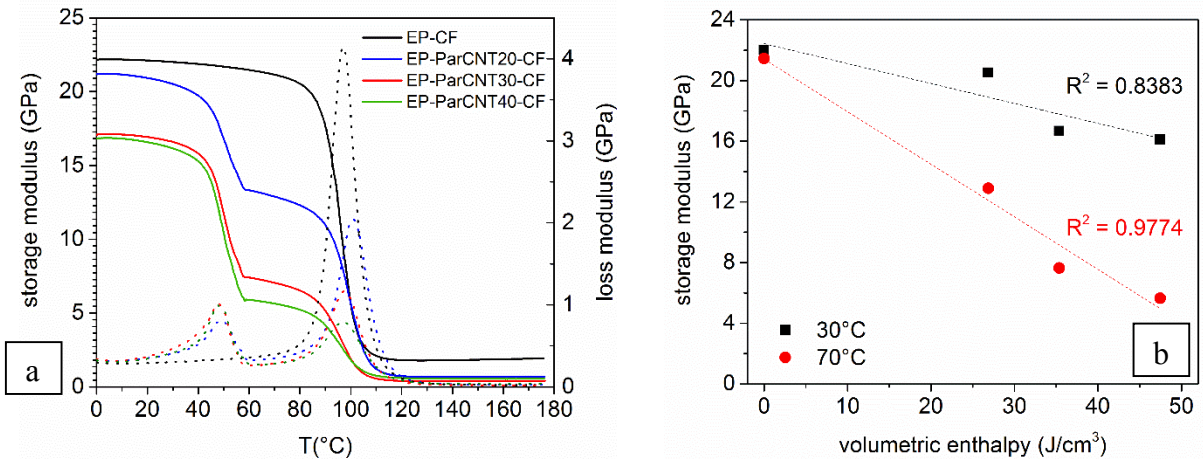

Figure 9. DMTA results. (a) Storage modulus and loss modulus as a function of temperature. (b) storage modulus at 30°C and 70°C as a function of the volumetric melting enthalpy of the laminates (see Table 4).

This test evidences all the transitions the samples undergo in the considered temperature range. For all the samples, the storage modulus (E') presents a sharp decrease in correspondence of the glass transition temperature of the epoxy resin. As reported in DSC tests, the position of

the T_g, here determined in correspondence of the loss modulus (E") peak, is not substantially affected by the presence of paraffin inside the laminates. The laminates containing paraffin present an additional signal in both E' and E" curves at approximately 50 °C, due to the melting of the PCM. The two transitions are detectable also in the trend of the loss moduli, which present peaks at the melting temperature of the paraffin and at the T_g of the epoxy. However, an important reduction of E' can be detected over the entire testing interval upon paraffin addition.

3.4 Mechanical analysis

Representative load-displacement curves obtained in flexural tests are reported in Figure 10.

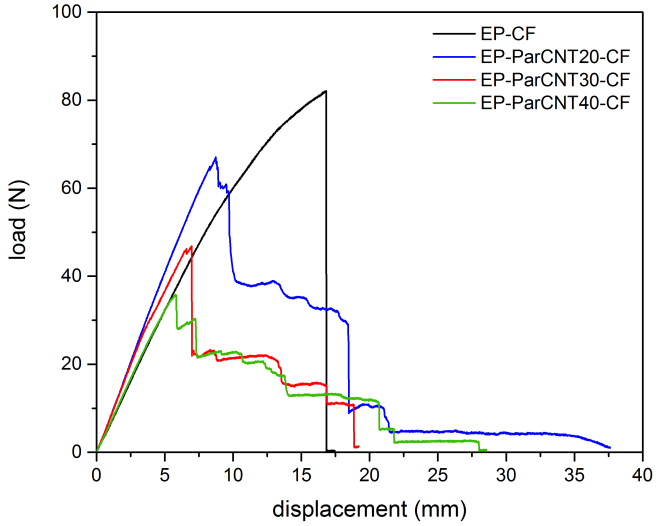

Figure 10. representative load-displacement curves obtained from three-point bending tests.

In all cases, the curves present an initial linear region, followed by a region where the slope decreases before the maximum load is reached. After the maximum load, the behavior of the EP-CF laminates is remarkably different from those containing the PCM particles. For EP-CF laminates, the load reaches a maximum value and suddenly drops to zero, and the specimens break with a catastrophic failure. This was observed for all the tested specimens, and suggests the

presence of a quite strong interlaminar adhesion [37, 43, 44] . On the other hand, the samples containing paraffin show a progressive failure, and the load-displacement curves present a sequence of drops and plateaus. Thus, the specimens absorb mechanical energy also during the damage propagation. Also, the maximum load is decreasing as the PCM content in the laminates increases. From a visual observation of the specimens during the test, it was seen that in EP-CF laminate the failure starts from the mid lower region of the specimen, subjected to tensile stress, and quickly propagates through the thickness, while for the laminates with ParCNT the failure is a combination of delamination and damage in the mid upper zone, subjected to compression. This failure mode, associated with a multistage failure in bending, was previously reported in the literature for woven fabric reinforced composites [37]. The presence of delamination in the early stages of failure suggests that the tensile strength is remarkably higher than the in-plane shear strength of the laminates with PCM. The most important mechanical parameters measured in bending tests are summarized in Table 5. The flexural modulus decreases only slightly with the increase of the PCM content. This result was expected, since the flexural modulus is evaluated at low deformations and strongly depends on the volume fraction of the reinforcement phase [37], which is almost the same for the investigated composites. Although the presence of delamination can reduce the elastic modulus [35], this is likely not the case in the present work, because the delamination mechanisms were observed to start at deflection values higher than those considered for measuring the elastic modulus. This suggests that the chosen span-to-thickness ratio was sufficiently high to correctly evaluate the elastic modulus. The fact that the modulus does not decrease with the PCM content is positive for the development of composites in which both high stiffness and thermal energy storage capabilities are combined. However, the appearance of these new failure mechanisms is most probably the cause of the decrease of both flexural strength and strain at break values (Table 5) with the PCM content. It should be noted

that, as already mentioned (paragraph 2.3.4), the calculated value of σ_{fM} represents an apparent flexural strength, because the stress is not linear through the thickness and because, since the failure is not due to the pure bending moment, the calculated stress differs from the real stress in the mid lower portion of the specimen, subjected to the highest tensile stress [30]. Nevertheless, these tests clearly highlight the differences in the failure mode and in the behavior during the damage propagation, after the maximum load is reached. To investigate the effect of PCM introduction on the interlaminar shear strength of the laminates, short-beam shear tests were performed. The obtained values of short-beam interlaminar shear strength, F^{sbs}, are reported in Table 5.

Table 5. Mechanical parameters obtained from three-point bending tests and the short-beam shear tests on the laminates.

Sample	E (GPa)	σ_{fM} (MPa)	ε_b (%)	F^{sbs} (MPa)
EP-CF	35.8 ± 1.5	705 ± 57	2.25 ± 0.15	50.8 ± 0.9
EP-ParCNT20-CF	31.6 ± 2.0	283 ± 49	1.15 ± 0.11	30.0 ± 2.7
EP-ParCNT30-CF	29.7 ± 3.9	222 ± 10	0.91 ± 0.09	22.9 ± 2.9
EP-ParCNT40-CF	29.5 ± 3.2	197 ± 14	0.77 ± 0.02	13.2 ± 0.8

The results are in good agreement with the three-point bending tests, since the values of F^{sbs} decrease almost linearly with the PCM content in the matrix. This is probably due to the uneven distribution of the PCM; in both optical microscopy and SEM observations (Figures 2 and 3), it appears that the PCM particles concentrate in the interlaminar zone while only the epoxy phase infiltrates the tows. This is believed to reduce the interlaminar shear strength of the laminates, as the PCM phase could create a preferential site for damage propagation, since it is formed by

paraffin wax and CNTs and has a low strength and ductility. During short-beam shear tests, many mechanisms of failure can generally be observed, such as delamination in several planes, failure in compression or in tension due to the bending moment, damages due to the stresses applied by the loading nose and the supports on the lower face, crushing of the specimens between the nose and the supports, etc. [31, 45]. Some of these phenomena were also observed during the present study, at the final stages of the test. However, the main observed failure mode, corresponding to the first drop in the load, was associated to delamination. Thus, although the reported values of F^{sbs} may not coincide with the real interlaminar shear strength of the composite, they are still important for a comparison of the shear properties of the different laminates [34].

4. Conclusions

Novel multifunctional structural composite laminates with thermal energy storage (TES) capability were developed by combining a paraffinic PCM stabilized with CNTs, an epoxy resin and a carbon fiber fabric. The fiber content and pore fractions were similar for the prepared laminates at different compositions, which allowed a consistent evaluation of their physical properties. DSC revealed that the paraffin keeps its thermal properties also in the laminates, and the melting enthalpy of the composites was almost proportional to the paraffin weight fraction. The thermal properties of the laminates were retained even after fifty thermal cycles. Moreover, the thermal conductivity increased proportionally to the content of stabilized PCM. This effect could be attributed to the presence of CNTs as a stabilizing filler in the PCM domains. The positive contribute of the developed TES laminates to the thermal energy management was also proven by monitoring their cooling rates through thermal imaging.

Three-point bending test showed that the flexural modulus was only slightly impaired by the presence of PCM, while the flexural strength and the strain at break were significantly reduced.

For example, for the EP-ParCNT40-CF sample, which was the least performant in the mechanical tests, the flexural strength and the strain at break were the 30 % and the 35 % of the values shown by the laminate without ParCNT. The interlaminar shear strength was also negatively affected by PCM addition. As revealed by optical microscope images, it could be attributed to the preferential location of the PCM in the interlaminar region rather than between the fibers of the same tow. This work demonstrates the possibility to design multifunctional structural TES composites, and further efforts will be devoted to improving the PCM distribution within the laminates and their mechanical properties.

Acknowledgements

Dr. Seraphin Unterberger (AB Materialtechnologie - Inst. für Konstruktion und Materialwissenschaften, Innsbruck, Austria) is gratefully acknowledged for his precious support with the laser flash analysis measurements.

References

[1] Fleischer A. Thermal energy storage using phase change materials. Fundamentals and applications: Springer; 2015.

[2] Hasnain SM. Review on sustainable thermal energy storage technologies, Part I: heat storage materials and techniques. Energy Conversion and Management. 1998;39(11):1127-1138.

[3] Pielichowska K, Pielichowski K. Phase change materials for thermal energy storage. Progress in materials science. 2014;65:67-123.

[4] Khudhair AM, Farid MM. A review on energy conservation in building applications with thermal storage by latent heat using phase change materials. Energy Conversion and Management. 2004;45(2):263-275.

[5] Kalaiselvam S, Parameshwaran R. Thermal Energy Storage Technologies for Sustainability. Chapter 5: Latent thermal energy storage: Elsevier; 2014.

[6] Khadiran T, Hussein MZ, Zainal Z, Rusli R. Encapsulation techniques for organic phase change materials as thermal energy storage medium: A review. Sol Energy Mater Sol Cells. 2015;143:78-98.

[7] Jeong S-G, Kim S, Huh W. Preparation of epoxy resin using n -hexadecane based shape stabilized PCM for applying wood-based flooring. Journal of Adhesion Science and Technology. 2014;28(7):711-721.

[8] Zhang P, Xiao X, Ma ZW. A review of the composite phase change materials: Fabrication, characterization, mathematical modeling and application to performance enhancement. Applied Energy. 2016;165:472-510.

[9] Khadiran T, Zobir M, Zainal Z, Rusli R. Advanced energy storage materials for building applications and their thermal performance characterization : A review. Renewable and Sustainable Energy Reviews. 2016;57:916-928.

[10] Pielichowska K, Bieda J, Szatkowski P. Polyurethane/graphite nano-platelet composites for thermal energy storage. Renewable Energy. 2016;91:456-465.

[11] Cui Y, Xie J, Liu J, Pan S. Review of Phase Change Materials Integrated in Building Walls for Energy Saving. Procedia Engineering. 2015;121:763-770.

[12] Dorigato A, Ciampolillo MV, Cataldi A, Bersani M, Pegoretti A. Polyethylene wax/EPDM blends as shape-stabilized phase change materials for thermal energy storage. Rubber Chemistry and Technology. 2017;90(3):575-584.

[13] Cabeza LF, Ibáñez M, Solé C, Roca J, Nogués M. Modelization of a water tank including a PCM module. Applied Thermal Engineering. 2006;26(11-12):1328-1333.

[14] Kürklü A, Özmerzi A, Bilgin S. Thermal performance of water-phase change material solar collector. Renewable Energy. 2002;26(3):391-399.

[15] Farid MM, Khudhair AM, Razack SAK, Al-Hallaj S. A review on phase change energy storage: Materials and applications. Energy Conversion and Management. 2004;45(9-10):1597-1615.

[16] Dorigato A, Canclini P, Unterberger SH, Pegoretti A. Phase changing nanocomposites for low temperature thermal energy storage and release. Express Polymer Letters. 2017;11(9):738-752.

[17] Onder E, Sarier N, Cimen E. Encapsulation of phase change materials by complex coacervation to improve thermal performances of woven fabrics. Thermochimica Acta. 2008;467:63-72.

[18] Shin Y, Yoo DI, Son K. Development of thermoregulating textile materials with microencapsulated Phase Change Materials (PCM). II. Preparation and application of PCM microcapsules. Journal of Applied Polymer Science. 2005;96(6):2005-2010.

[19] Fok SC, Shen W, Tan FL. Cooling of portable hand-held electronic devices using phase change materials in finned heat sinks. International Journal of Thermal Sciences. 2010;49(1):109-117.

[20] Carlson T. Multifunctional Composite Materials. Design, Manufacture and Experimental Characterisation. Doctoral thesis. Luleå University of Technology, Department of Engineering Sciences and Mathematics, Materials Science, 2013.

[21] Gibson RF. A review of recent research on mechanics of multifunctional composite materials and structures. Composite Structures. 2010;92(12):2793-2810.

[22] Salonitis K, Pandremenos J, Paralikas J, Chryssolouris G. Multifunctional materials: Engineering applications and processing challenges. International Journal of Advanced Manufacturing Technology. 2010;49(5-8):803-826.

[23] Chawla KK. Composite materials: science and engineering. Chapter 3: Polymer matrix composites. Third edit ed. New York, USA: Springer; 2013.

[24] Wirtz R, Fuchs A, Narla V, Shen Y, Zhao T, Jiang Y. A Multi-functional graphite/epoxy-based thermal energy storage composite for temperature control of sensors and electronics. University of Nevada, Reno Reno, Nevada, 89557 USA2003. p. 1-9.

[25] Yoo S, Kandare E, Shanks R, Al-Maadeed MA, Afaghi Khatibi A. Thermophysical Properties of Multifunctional Glass Fibre Reinforced Polymer Composites Incorporating Phase Change Materials. Thermochimica Acta. 2016;642:25-31.

[26] Yoo S, Kandare E, Mahendrarajah G, Al-Maadeed MA, Khatibi AA. Mechanical and thermal characterisation of multifunctional composites incorporating phase change materials. J Compos Mater. 2017;51(18):2631-2642.

[27] Fredi G, Dorigato A, Fambri L, Pegoretti A. Wax confinement with carbon nanotubes for phase changing epoxy blends. Polymers. 2017;9(9):405-420.

[28] Soliman E, Kandil U, Taha MR. Improved Strength and Toughness of Carbon Woven Fabric Composites with Functionalized MWCNTs. Materials 2014;7:4640-4657.

[29] Standard Test Methods for Density and Specific Gravity (Relative Density) of Plastics by Displacement. ASTM D792 − 13., 2013.

[30] Dong C, Davies IJ. Flexural strength of bidirectional hybrid epoxy composites reinforced by E glass and T700S carbon fibers. Composites B. 2015;72:65-71.

[31] Cui W, Wisnom MR, Jones M. Effect of specimen size on interlaminar shear strength of unidirectional carbon fibre-epoxy. Composites Engineering. 1994;4(3):299-307.

[32] Selmi A. Void Effect on Carbon Fiber Epoxy Composites. 2nd International Conference on Emerging Trends in Engineering and Technology (ICETET'2014), London, UK2014.

[33] Michaud D, Sequeira Tavares S, Sigg A, Lavanchy S, Månson J-AE. Low pressure processing of high fiber content composites The 8th International Conference on Flow Processes in Composite Materials (FPCM8) Douai, FRANCE2006. p. 393-400.

[34] Deng S, Ye L, Mai Y-W. Influence of fiber cross-sectional aspect ratio on mechanical properties of glass-fiber/epoxy composites II. Interlaminar fracture and impact behaviour. Composites Science and Technology. 1999;59:1725-1734.

[35] Sudarisman, Davies IJ. Flexural failure of unidirectional hybrid fibre-reinforced polymer (FRP) composites Containing Different Grades of Glass Fibre. Advanced Materials Research. 2008;41-42:357-362.

[36] Poyyathappan K, Bhaskar GB, Pazhanivel K, Venkatesan N. Tensile and flexural studies on glass-carbon hybrid composites subjected to low frequency cyclic loading. International Journal of Engineering and Technology (IJET). 2014;6(1):83-90.

[37] Abdel Ghafaar M, Mazen AA, El-Mahallawy NA. Behavior of woven fabric reinforced epoxy composites under bending and compressive loads. Journal of Engineering Sciences. 2006;34(2):453-469.

[38] Luyt AS, Krupa I. Phase change materials formed by uv curable epoxy matrix and Fischer-Tropsch paraffin wax. Energy Conversion and Management. 2009;50(1):57-61.

[39] Zhang P, Hu Y, Song L, Ni J, Xing W, Wang J. Effect of expanded graphite on properties of high-density polyethylene/paraffin composite with intumescent flame retardant as a shape-stabilized phase change material. Sol Energy Mater Sol Cells. 2010;94(2):360-365.

[40] Kandare E, Khatibi AA, Yoo S, Wang R, Ma J, Olivier P, et al. Improving the through-thickness thermal and electrical conductivity of carbon fibre/epoxy laminates by exploiting synergy between graphene and silver nano-inclusions. Composites Part A: Applied Science and Manufacturing. 2015;69:72-82.

[41] Yu G-C, Wu L-Z, Feng L-J. Enhancing the thermal conductivity of carbon fiber reinforced polymer composite laminates by coating highly oriented graphite films. Materials & Design. 2015;88:1063-1070.

[42] Fang X, Fan L-W, Ding Q, Yao X-L, Wu Y-Y, Hou J-F, et al. Thermal energy storage performance of paraffin-based composite phase change materials filled with hexagonal boron nitride nanosheets. Energy Conversion and Management. 2014;80:103-109.

[43] Ary Subagia IDG, Kim Y, Tijing LD, Sang Kim C, Kyong Shon H. Effect of stacking sequence on the flexural properties of hybrid composites reinforced with carbon and basalt fiber. Composites: Part B 2014;58:251-258.

[44] Pegoretti A, Cristelli I, Migliaresi C. Experimental optimization of the impact energy absorption of epoxy-carbon laminates through controlled delamination. Composites Science and Technology. 2008;68(13):2653–2662.

[45] Standard Test Method for Short-Beam Strength of Polymer Matrix Composite Materials and Their Laminates. ASTM D 2344/D 234M - 00. 2006.